Chinese Chemical Letters 37 (2026) 111649

Contents lists available at ScienceDirect

Chinese Chemical Letters

journal homepage: www.elsevier.com/locate/cclet

Handheld integrated needle sensor based on arginine-engineered Cu-MOF with boosted enzyme-mimicking activity for sensitive detection of glyphosate

Yifei Chen[a], Yu Wu[a], Weiqing Xu[a], Yinjun Tang[a], Yujia Cai[a], Wenhong Yang[a], Wenxuan Jiang[a], Xin Yu[a], Jian Li[a], Ying Zhou[a], Yiwei Qiu[a], Wenling Gu[a], Chengzhou Zhu[a,b,*]

[a] State Key Laboratory of Green Pesticide, International Joint Research Center for Intelligent Biosensing Technology and Health, College of Chemistry, Central China Normal University, Wuhan 430079, China
[b] College of Material Chemistry and Chemical Engineering, Key Laboratory of Organosilicon Chemistry and Material Technology, Ministry of Education, Hangzhou Normal University, Hangzhou 311121, China

ARTICLE INFO

Article history:
Received 17 March 2025
Revised 17 June 2025
Accepted 30 July 2025
Available online 7 August 2025

Keywords:
Enzyme-like catalysis
Functional modulator
Metal-organic frameworks
Sensing
Glyphosate

ABSTRACT

Metal-organic frameworks (MOFs) with tunable structures provide a versatile platform for exploring active sites and show great potential in enzyme-like catalysis. In this study, arginine was employed as a modulator to synthesize an arginine-copper metal-organic framework (Arg-Cu-MOF), which demonstrated superior peroxidase-like activity and stability in comparison to unmodified Cu-MOF. The improved activity resulted from an increased density of Cu^+ active sites, facilitating efficient $^{\bullet}OH$ generation through H_2O_2 decomposition. Glyphosate interacts with the copper sites in a way that affects $^{\bullet}OH$ generation and chromogenic substrate oxidation, leading to detectable colorimetric changes. By integrating Arg-Cu-MOF into a needle sensor, we allowed sample handling, reagent mixing, and signal readout, enabling both precise instrumental measurements and semi-quantitative visual detection of glyphosate. This sensor offers a detection range of 0.05–200 μg/mL with a detection limit of 0.049 μg/mL. This work highlights the potential of MOF modulation strategies and integrated detection platforms to enhance analytical performance, improve user-friendliness, and expand the application scope of biomimetic nanomaterials.

© 2026 Published by Elsevier B.V. on behalf of Chinese Chemical Society and Institute of Materia Medica, Chinese Academy of Medical Sciences.

Metal-organic frameworks (MOFs) are promising candidates for enzyme-like catalysis due to their structural tunability, large surface area, and ability to host active sites for redox reactions [1–6]. The highly ordered porous structure of MOFs facilitates substrate accessibility and allows for the incorporation of various catalytic centers, such as metal ions and organic linkers [7–9]. However, achieving high catalytic activity in MOFs and expanding their sensing applications remain significant challenges. These limitations primarily stem from the intrinsic crystalline nature of MOFs, where metal nodes are often embedded within the framework, reducing their availability for catalytic reactions. Traditional synthesis approaches typically prioritize structural stability and porosity, often at the expense of catalytic efficiency. This trade-off underscores the need for innovative strategies to increase active site exposure while maintaining the structural integrity of MOFs.

Various strategies have been explored to enhance the catalytic sensing performance of MOFs, including post-synthetic modification, metal node engineering, and the introduction of functional ligands [10–13]. Among these, the introduction of modulators during synthesis has emerged as a particularly effective method for fine-tuning structural and catalytic properties [14–17]. However, MOF-based sensors encounter limitations in practical applications. Their porous structures often hinder access to catalytic active sites, limiting their effectiveness in detecting trace analytes. Additionally, their fragile frameworks are susceptible to degradation, particularly during repeated use in complex environments [18–21]. These issues often stem from limited access to catalytically active sites and the weakening of the framework during repeated use in complex environments [22–27]. Furthermore, existing modulation strategies frequently encounter a trade-off, where enhancing active site exposure for better sensitivity compromises structural integrity, and *vice versa* [28–31]. Addressing this conflict is crucial for advancing MOF-based catalytic sensing systems, where both high sensitivity and stability are indispensable [32,33].

* Corresponding author.
E-mail address: czzhu@ccnu.edu.cn (C. Zhu).

https://doi.org/10.1016/j.cclet.2025.111649
1001-8417/© 2026 Published by Elsevier B.V. on behalf of Chinese Chemical Society and Institute of Materia Medica, Chinese Academy of Medical Sciences.

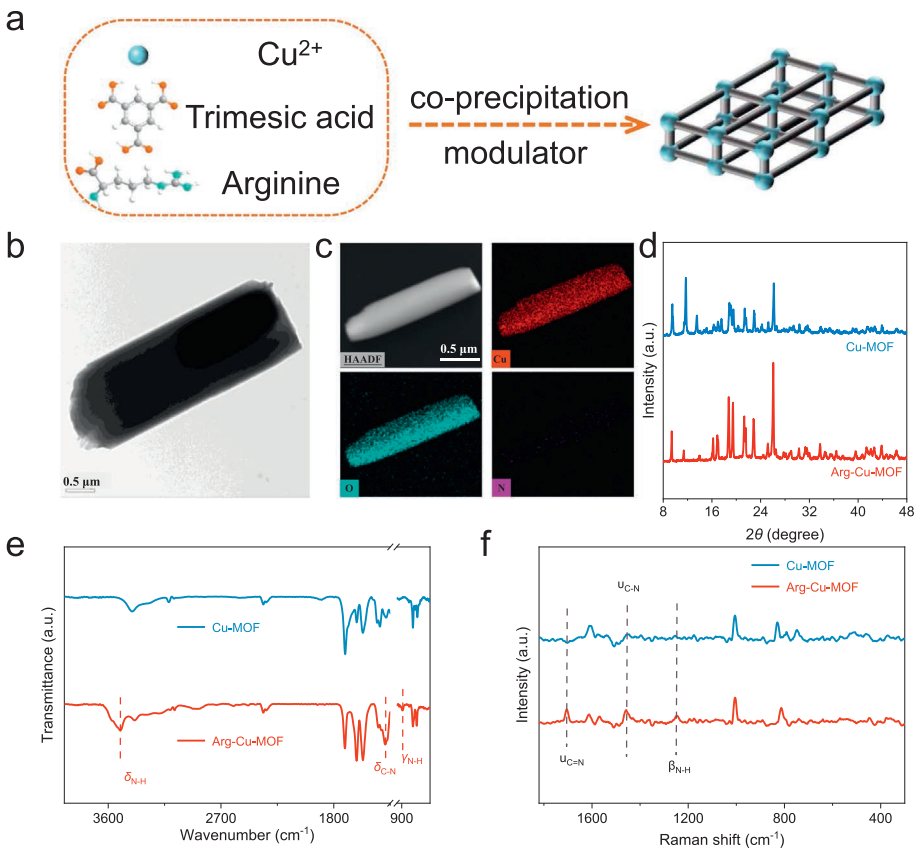


Fig. 1. (a) Illustration of the preparation process of Arg-Cu-MOF. (b) TEM image of Arg-Cu-MOF. (c) HAADF-STEM image and STEM-EDS mappings of Arg-Cu-MOF. (d) Powder XRD patterns, (e) FT-IR spectra, and (f) Raman spectra of Cu-MOF and Arg-Cu-MOF.

In this study, we utilized arginine as a modulator to enhance the enzyme-like activity and stability of the copper metal-organic framework (Cu MOF). Its incorporation during synthesis strengthened the framework structure, markedly increasing the accessibility of active sites and boosting peroxidase (POD)-like activity by promoting more efficient ·OH generation. This modification led to a 4.97-fold increase in catalytic activity compared to the unmodified Cu MOF. Notably, the Arg-Cu-MOF exhibited superior catalytic efficiency under neutral pH conditions, highlighting its potential for practical applications. By leveraging the interaction between glyphosate and copper ions to effectively inhibit the colorimetric reaction, we achieved sensitive glyphosate detection with a detection range of 0.05–200 μg/mL and a detection limit of 0.049 μg/mL. Additionally, the Arg-Cu-MOF was incorporated into a syringe-based device, demonstrating a practical application for glyphosate detection. This work highlights the potential of modulator-driven MOF design in addressing sensitivity and stability, paving the way for reliable and high-performance catalytic sensing systems.

The Cu-MOF with POD-like activity was selected as a model, and arginine was introduced as the dual-function modulator to enrich the metal sites and improve the stability of the resulting Arg-Cu-MOF (Fig. 1a). Transmission electron microscopy (TEM) was employed to characterize the morphology of Arg-Cu-MOF and Cu-MOF. As shown in Fig. 1b and Fig. S1a (Supporting information), the Arg-Cu-MOF exhibits a rectangle-shaped plate-like morphology distinct from the rod-like structure of the original Cu-MOF. Energy-dispersive spectroscopy (EDS) confirmed the uniform distribution of Cu and O elements in both Arg-Cu-MOF and Cu-MOF (Fig. 1c and Fig. S1b in Supporting information). Furthermore, the presence of N in Arg-Cu-MOF confirms the successful introduction of arginine. The powder X-ray diffraction (XRD) patterns (Fig. 1d) reveal no significant differences between Arg-Cu-MOF and Cu-MOF, indicating that arginine introduction does not disrupt the crystal structure. Additional spectral analyses corroborate the presence of arginine in the MOF framework. The Fourier transform infrared (FT-IR) spectrum (Fig. 1e) displays peaks at 1507, 1393, and 888 cm^{-1} corresponding to δ(N-H), δ(C-N), and γ(C-N) modes, respectively, confirming arginine incorporation [34,35]. Similarly, the ^{1}H NMR spectrum (Fig. S2) (Supporting information) confirms the involvement of arginine in the MOF synthesis [36]. Finally, the Raman spectrum (Fig. 1f) shows the peaks at 1703, 1568, and 1250 cm^{-1}, attributed to ν(C=N), ν(C-N), and β(N-H) modes, respectively, providing further evidence of arginine integration.

The inductively coupled plasma mass spectrometry (ICP-MS) analysis (Table S1 in Supporting information) reveals that Arg-Cu-MOF contains 27.72 wt% of copper, a significant increase compared to the 18.10 wt% in Cu-MOF, highlighting the enhancement in Cu sites and catalytic performance. Similarly, energy-dispersive X-ray spectroscopy (EDS) results (Fig. 2a) further confirm the trend, showing an increased Cu signal intensity in Arg-Cu-MOF compared to Cu-MOF. To further investigate the elemental composition and valence states of Arg-Cu-MOF, X-ray photoelectron spectroscopy (XPS) was conducted. As displayed in Fig. S3, the survey spectrum of Arg-Cu-MOF indicates the existence of Cu, N, O, and C. The high-resolution Cu 2p spectrum shown in Fig. 2b reveals two types of copper species, with the peak at 933.6 eV attributed to Cu^+ [37,38]. Arginine incorporation leads to unsaturated coordination at Cu sites, increasing the Cu^+ content in Arg-Cu-MOF from 31% to 42% and thus enhancing its catalytic activity [39,40]. Furthermore, the XPS spectra of O 1s and C 1s (Fig. S4 in Supporting information) confirm the higher abundance of Cu-O bonds in Arg-Cu-MOF. Thermogravimetric analysis (TGA) and differential ther-

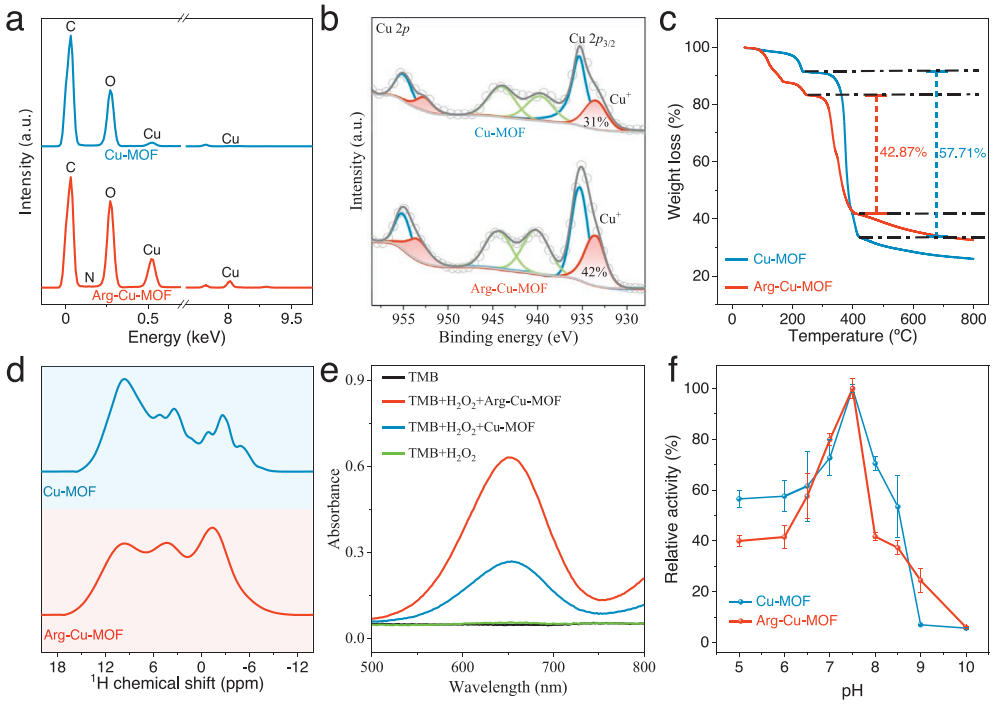


Fig. 2. (a) EDS spectra of Cu-MOF and Arg-Cu-MOF. (b) High-resolution Cu 2p XPS spectra of Arg-Cu-MOF and Cu-MOF (Inset: the corresponding relative contents of different Cu species of the Arg-Cu-MOF and Cu-MOF). (c) TGA curves of Arg-Cu-MOF and Cu-MOF. (d) ^{1}H NMR spectra of Arg-Cu-MOF and Cu-MOF. (e) Absorption spectra of TMB catalyzed by the Cu-MOF and Arg-Cu-MOF with H_2O_2 in Tris–HCl (pH 7.5). (f) Relative activities of Cu-MOF and Arg-Cu-MOF treated with different pH values.

mogravimetry curve (DTG) (Fig. 2c and Fig. S5 in Supporting information) reveal that the removal rate of coordinating molecules in Arg-Cu-MOF is 42.87 % within the temperature range of 243 °C to 417 °C, which is significantly lower than the 57.71 % observed for Cu-MOF [41,42]. This suggests that the modulator enhances stability by strengthening the binding between coordinating molecules and metal nodes in the material. The solid-state nuclear magnetic resonance characterization (Fig. 2d) reveals that the Cu-MOF exhibits multiple split resonance signals in the aromatic region (6–12 ppm), indicating heterogeneous aromatic environments and structural irregularities within the framework. In contrast, Arg-Cu-MOF shows significantly improved spectral resolution, with well-defined, sharp resonance patterns and uniform peak profiles across the chemical shift domains [43–45]. This change suggests that the incorporation of arginine not only enhances the order of aromatic ligands but also improves the structural regularity of the entire MOF, thereby improving the stability of the framework. To assess the structural impact of arginine as a modulator, the Brunauer-Emmett-Teller (BET) surface area and porosity of Cu-MOF and Arg-Cu-MOF were analyzed. The N_2 uptake decreases with the addition of the modulator arginine. As shown in Fig. S6 (Supporting information), the BET surface area of the Arg-Cu-MOF was measured at 28.09 m^2/g, lower than the 65.67 m^2/g observed for the unmodified. This reduction suggests that arginine likely promotes structural densification of Arg-Cu-MOF, potentially enhancing its stability and reducing excessive porosity. The observed decrease in BET surface area may reflect a shift towards a more compact framework, which could improve material robustness while maintaining sufficient accessibility for catalytic sites [46,47].

The POD-like activity of Arg-Cu-MOF was assessed by monitoring the colorimetric reaction of TMB in the presence of H_2O_2. As depicted in Fig. 2e, the Arg-Cu-MOF reaction system exhibits a strong response at 652 nm compared to Cu-MOF, indicating that the POD-like activity of Arg-Cu-MOF is significantly enhanced upon the introduction of arginine. It is worth noting that the TMB solution containing only Arg-Cu-MOF exhibited almost no color change and showed low absorption at 652 nm (Fig. S7 in Supporting information), indicating that Arg-Cu-MOF has very weak and negligible oxidase-like activity. Furthermore, Arg-Cu-MOF demonstrated low catalase-like activity as well (Fig. S8 in Supporting information). These results suggest that Arg-Cu-MOF possesses POD-like activity with good specificity. To investigate the effect of pH on the POD-like activity of Arg-Cu-MOF, the POD-like activity was measured by varying the pH from 5 to 10, while keeping the concentrations of Arg-Cu-MOF, H_2O_2, and TMB constant. As illustrated in Fig. 2f, the POD-like activity of Arg-Cu-MOF reaches its maximum at pH 7.5, which may be attributed to the optimal structural integrity under this condition. Additionally, as shown in the zeta potential measurements (Fig. S9 in Supporting information), Arg-Cu-MOF exhibits a more negative zeta potential (−21.28 mV) in neutral buffer compared to acidic conditions (−4.34 mV). The more negative zeta potential suggests stronger electrostatic repulsion, enhancing colloidal stability and preventing aggregation, thereby exposing more active sites for catalysis. In addition, the use of neutral buffers minimizes corrosive effects on MOFs, enhancing durability and detection performance while ensuring environmental and biological compatibility. Consistently, SEM images, XRD, and dynamic light scattering (DLS) analyses under different pH conditions (Figs. S10 and S11 in Supporting information) further confirm that Arg-Cu-MOF maintains superior structural stability at pH 7.5.

To understand the catalytic efficiency and mechanism, the steady-state kinetic assays of Arg-Cu-MOF and Cu-MOF were carried out. As shown in Figs. S12 and S13 (Supporting information), the data align with typical Michaelis-Menten and Lineweaver-Burk models. Other detailed parameters, including kinetic parameters such as K_m and V_{max}, are listed in Table S2. Compared to the natural horseradish peroxidase (HRP) and other materials, the lower K_m and higher V_{max} of Arg-Cu-MOF demonstrate the superiority of this POD-like performance. Notably, the V_{max} of Arg-Cu-MOF is 4.97 times greater than that of Cu-MOF, indicating significantly enhanced catalytic velocity. To further investigate the POD-like activity of Arg-Cu-MOF, electron paramagnetic resonance (EPR) and

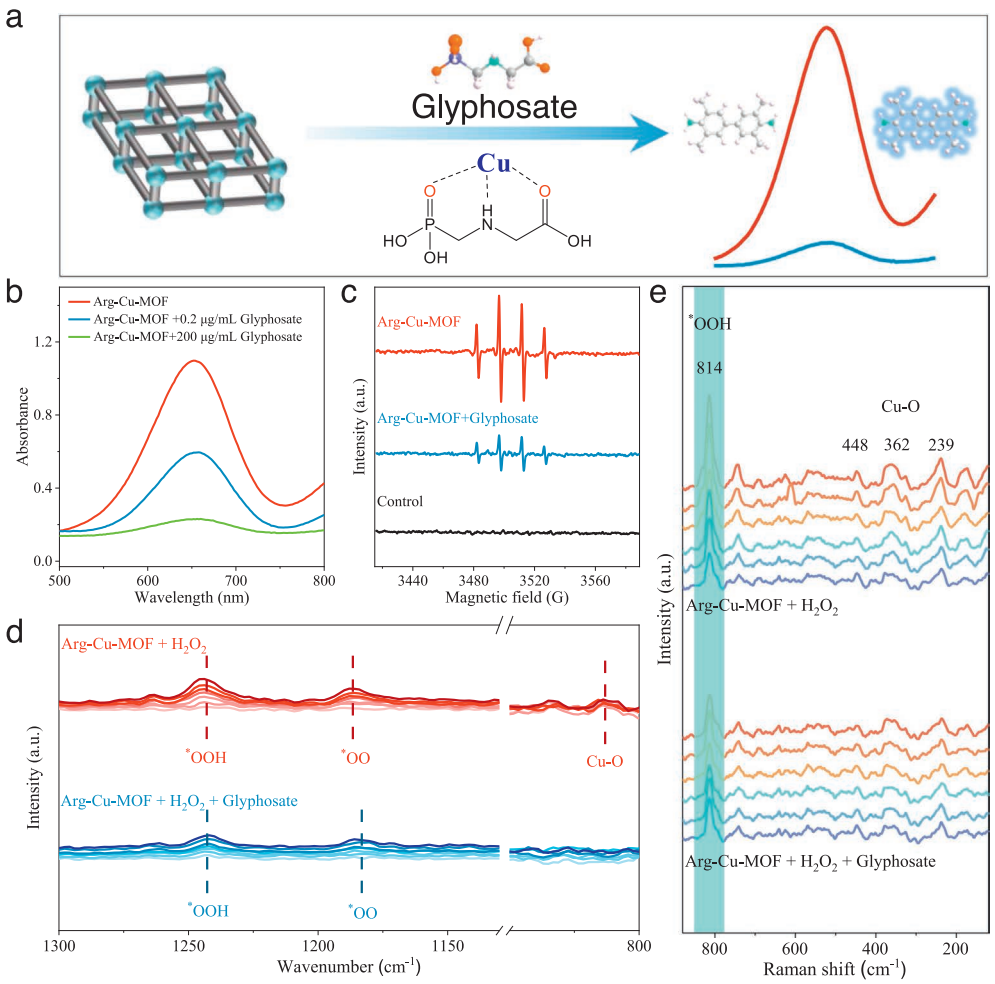


Fig. 3. (a) Schematic diagram of Arg-Cu-MOF detection of glyphosate. (b) Absorption spectra of TMB catalyzed by the Arg-Cu-MOF with glyphosate in Tris–HCl (pH 7.5). (c) DMPO spin trapping EPR spectra of Arg-Cu-MOF and Arg-Cu-MOF + glyphosate system. (d) *In situ* ATR-FTIR spectra and (e) *in situ* Raman spectra of Arg-Cu-MOF and Arg-Cu-MOF + glyphosate system.

trapping experiments were conducted to detect potential reactive oxygen species. Using 5,5-dimethyl-1-pyrroline *N*-oxide (DMPO) as a trapping agent, the typical signals of the DMPO-•OH adduct indicate the existence of hydroxyl radicals (•OH) (Fig. S14 in Supporting information). Additionally, Fig. S15 (Supporting information) presents the absorption spectra of TMB catalyzed by Cu^{2+} and Cu^{+} with H_2O_2, demonstrating that Cu^{+} possesses superior catalytic activity. Arg-Cu-MOF exhibits a stronger •OH signal than Cu-MOF, which can be attributed to the higher Cu^{+} content in Arg-Cu-MOF [48]. This increased Cu^{+} content promotes the generation of more free radicals, thereby accelerating the reaction.

Glyphosate is the most widely used herbicide worldwide, effectively controlling weed growth, yet its environmental residues and potential ecological health risks have sparked significant concerns. Given its persistence in soil and water and possible ecosystem impacts, developing efficient and sensitive glyphosate detection methods is essential for food safety [49–51]. Glyphosate effectively inhibits the colorimetric reaction facilitated by Cu-MOF, likely through interactions with copper ions. The Arg-Cu-MOF enhances coordination with glyphosate by increasing the exposure of metal active sites, which further lowers its POD-like activity. This strategy greatly enhances detection sensitivity, positioning Arg-Cu-MOF as an appealing candidate for the accurate detection of glyphosate (Fig. 3a). To verify this, UV-vis characterization of the Arg-Cu-MOF-H_2O_2-TMB system in the presence of glyphosate was conducted (Fig. 3b). Preincubation of glyphosate with Arg-Cu-MOF results in a noticeable decrease in the intensity of the characteristic absorption peak. Additionally, as the concentration of glyphosate increased, the peak intensity weakened further. EPR analysis also detected a variation in the generated •OH following the addition of glyphosate. The significant decrease in signal peak intensity confirms that glyphosate binds to the active sites, resulting in reduced POD-like activity in Arg-Cu-MOF (Fig. 3c). To investigate the catalytic process of Arg-Cu-MOF in the presence of glyphosate, *in situ* attenuated total reflectance Fourier-transform infrared (ATR-FTIR) spectroscopy was employed to monitor the reaction intermediates. Fig. 3d shows that the disappearance of the Cu-O peak at 820 cm^{-1} upon glyphosate introduction suggests an interaction between glyphosate and the copper active sites, resulting in the loss of this specific vibrational feature in Arg-Cu-MOF. Correspondingly, two infrared peaks at 1180 cm^{-1} and 1240 cm^{-1} are attributed to *OOH and *OO species on the copper active sites. After adding glyphosate, the rate of increase for the characteristic peaks of the adsorbed *OOH and *OO slows down, suggesting that glyphosate chelates with the active sites of Arg-Cu-MOF, thereby diminishing its catalytic capacity [52,53]. *In situ* Raman spectroscopy of Arg-Cu-MOF in the presence of glyphosate provided insight into changes in chemical composition at catalytic sites during H_2O_2 oxidation (Fig. 3e). Raman signals centering at 200–500 cm^{-1} can be attributed to the existence of Cu-O [54,55]. Notably, the Cu-O signal weakens in the Raman spectrum after the addition of glyphosate. This change indicates an interaction between glyphosate and the copper active

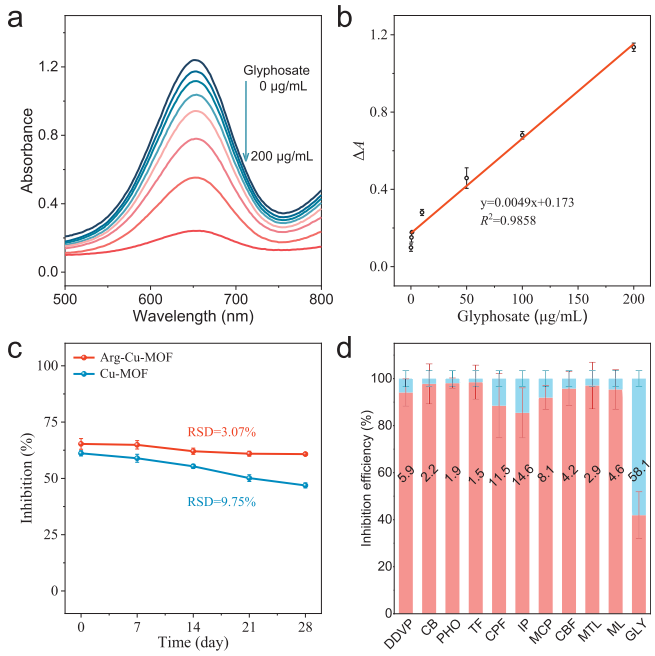


Fig. 4. (a) Absorption spectra of Arg-Cu-MOF in the presence of different glyphosate concentrations (Arg-Cu-MOF: 1 μg/mL). (b) Calibration curve of glyphosate detection. (c) Stability of Arg-Cu-MOF for the detection. (d) Selectivity test of Arg-Cu-MOF in the presence of interfering substances.

sites, which reduces the catalytic properties of Arg-Cu-MOF. Furthermore, the weakened signal at 814 cm^{-1} for *OOH supports this conclusion. SEM, XRD, and Cu 2p XPS analyses (Figs. S16 and S17 in Supporting information) also confirm that glyphosate inhibits the catalytic performance by binding to copper sites rather than by disrupting the structural integrity of the Arg-Cu-MOF.

The reaction solution from the sensor was first analyzed by UV-vis spectrophotometry (Figs. 4a and b). The results indicate that the absorbance value (ΔA) increases with concentration, exhibiting a significant linear relationship within the concentration range of 0.05–200 μg/mL. The corresponding linear regression equation is $\Delta A = 0.0049C + 0.173$ ($R^2 = 0.9858$) with the limit of detection (LOD) estimated to be 0.049 μg/mL ($3\sigma/k$, where k is the slope of the developed standard curve, and σ is the standard deviation of the nine blank samples). A comparison between the prepared sensor and previously reported methods for glyphosate detection is summarized in Table S3 (Supporting information). The device exhibits both a broader linear range and a lower detection limit. Furthermore, according to China's National Food Safety Standards, the detection range of the prepared sensor meets the requirements for practical application. To investigate the long-term stability of the Arg-Cu-MOF, it was stored for different days before being employed to detect glyphosate. As shown in Fig. 4c, the inhibition rate of Arg-Cu-MOF remained stable after 28 days of storage, with a relative standard deviation (RSD) of <3.07 %. In contrast, the inhibition rate for Cu-MOF fluctuated significantly over the same period, showing an RSD of 9.75 %. This result demonstrates that Arg-Cu-MOF offers superior stability compared to Cu-MOF. To evaluate the selectivity of the sensor, various pesticides were tested as potential interferents at a concentration of 1 mg/mL, including dichlorvos (DDVP), carbaryl (CB), phorate (PHO), trichlorfon (TF), chlorpyrifos (CPF), isocarbophos (IP), monocrotophos (MCP), carbofuran (CBF), methomyl (MTL), malathion (ML). In the presence of 0.1 mg/mL glyphosate, the inhibition rate for glyphosate was significantly higher than that of other pesticides (Fig. 4d). This result demonstrates the high selectivity of Arg-Cu-MOF for glyphosate. The accuracy and precision of the sensor for glyphosate detection

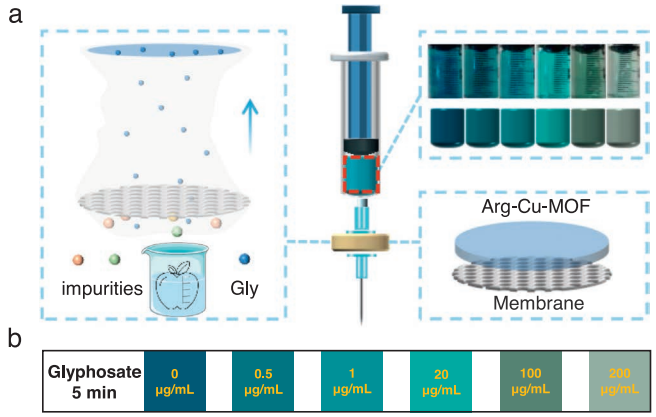


Fig. 5. (a) Arg-Cu-MOF reaction system in a syringe device. (b) Standard colorimetric card of glyphosate.

were evaluated through the recovery tests. As shown in Table S4 (Supporting information), the recovery of glyphosate measurement by the sensor is in the range of 99.81 % to 102.04 %, and the RSD is <2 %. These results confirm that the sensor provides high accuracy and precision, demonstrating its reliability for practical applications in glyphosate measurement.

In addition, as shown in Fig. 5a, a simple and portable visual semi-quantitative device for glyphosate detection has been designed. This handheld, needle-shaped colorimetric sensor integrates Arg-Cu-MOF-loaded glass cellulose, a filter membrane, and a chromogenic reagent. The device effectively filters out macromolecular particles such as dust, ensuring reliable and rapid glyphosate detection in fruits. Post-reaction images of standard glyphosate solutions were captured and analyzed to generate a colorimetric chart correlating glyphosate concentration with color intensity (Fig. 5b), enabling semi-quantitative detection. To evaluate the feasibility of the proposed handheld colorimetric sensor in real samples, fruit samples spiked with different concentrations of glyphosate were tested. In Table S5 (Supporting information), the results demonstrate that the color change observed aligns well with the outcomes from the established standard color chart, indicating that the developed handheld syringe-like sensor has practical application potential.

In conclusion, this study employed arginine as a modulator to enhance the POD-like activity and stability of Cu-MOF, achieving a 4.97-fold increase in catalytic efficiency compared to unmodified Cu-MOF. Systematic investigations revealed that arginine modulation improved the accessibility of active sites and optimized the coordination environment, enabling efficient •OH generation and superior catalytic performance under neutral pH conditions. Leveraging these, we developed a highly sensitive and selective sensor for glyphosate detection with a broad detection range (0.05–200 μg/mL) and an ultra-low detection limit (0.049 μg/mL). The integration of Arg-Cu-MOF into a syringe-based device enabled simultaneous sample handling, reagent mixing, and signal readout, facilitating both qualitative visual detection and precise quantitative analysis. This work not only provides valuable insights into MOF modulation strategies but also offers a practical, user-friendly solution for pesticide detection in food safety applications.

CRediT authorship contribution statement

Yifei Chen: Methodology, Formal analysis, Writing - original draft, Writing - review & editing. **Yu Wu:** Methodology, Formal analysis. **Weiqing Xu:** Resources, Data curation. **Yinjun Tang:** Methodology. **Yujia Cai:** Writing - review & editing. **Wenhong Yang:** Software. **Wenxuan Jiang:** Writing - review & editing. **Xin**

Yu: Writing - review & editing. **Jian Li:** Writing - review & editing. **Ying Zhou:** Writing - review & editing. **Yiwei Qiu:** Writing - review & editing. **Wenling Gu:** Supervision, Writing - review & editing. **Chengzhou Zhu:** Validation, Supervision, Writing - review & editing, Funding acquisition.

Declaration of competing interest

The authors declare that they have no known competing financial interests or personal relationships that could have appeared to influence the work reported in this paper.

Acknowledgments

The authors gratefully acknowledge the financial support from a start-up fund of Central China Normal University, the Fundamental Research Funds for the Central Universities (Nos. CCNU25QN004, CCNU24JCPT032 and CCNU22JC006), Natural Science Foundation of Hubei Province (No. 2023AFB571), Knowledge Innovation Program of Wuhan-Shuguang Project (No. 2023020201020441), the Open Research Fund of the Key Laboratory of Ministry of Education, Hangzhou Normal University (No. KFJJ2023009) and the Program of Introducing Talents of Discipline to Universities of China (111 program, No. B17019).

Supplementary materials

Supplementary material associated with this article can be found, in the online version, at doi:10.1016/j.cclet.2025.111649.

References

[1] K. Wang, J. Zhang, Y. Hsu, et al., Chem. Rev. 123 (2023) 5347–5420.
[2] Y. Wei, M. Zhang, R. Zou, et al., Chem. Rev. 120 (2020) 12089–12174.
[3] W. Xu, Y. Wu, W. Gu, et al., Chem. Soc. Rev. 53 (2024) 137–162.
[4] Y. Xu, A. Huang, W. Yi, et al., Coord. Chem. Rev. 500 (2024) 215517.
[5] X. Li, Z. Wang, J. He, et al., Chem. Sci. 16 (2025) 29–42.
[6] J. Chen, Y. Liu, Z. Long, et al., Chin. Chem. Lett. 35 (2024) 109463.
[7] J. Wu, Z. Wang, X. Jin, et al., Adv. Mater. 33 (2021) 2005024.
[8] M. Adeel, K. Asif, Md.M. Rahman, et al., Adv. Funct. Mater. 31 (2021) 2106023.
[9] Y. Chen, Y. Wu, W. Xu, et al., Anal. Chem. 96 (2024) 15231–15237.
[10] X. Yuan, X. Wu, J. Xiong, et al., Nat. Commun. 14 (2023) 1.
[11] X. Wang, X. Zhang, Y. Zhao, et al., Angew. Chem. Int. Ed. 62 (2023) e202310367.
[12] Z. Ye, Y. Jiang, L. Li, et al., eScience 3 (2023) 100107.
[13] X. Ma, H. Liu, W. Yang, et al., J. Am. Chem. Soc. 143 (2021) 12220–12229.
[14] M. Gao, L. Li, Z. Sun, et al., Angew. Chem. Int. Ed. 61 (2022) e202211216.
[15] D. Jiang, C. Huang, J. Zhu, et al., Coord. Chem. Rev. 444 (2021) 214064.
[16] M. Xu, D. Li, K. Sun, et al., Angew. Chem. Int. Ed. 60 (2021) 16372.
[17] B. Carpenter, A. Talosig, B. Rose, et al., Chem. Soc. Rev. 52 (2023) 6918–6937.
[18] T. Chen, H. Xu, S. Li, et al., Adv. Mater. 36 (2024) 2402234.
[19] W. Zhao, Y. Shi, Y. Jiang, et al., Angew. Chem. Int. Ed. 60 (2021) 5811.
[20] X. Huang, S. Zhang, Y. Tang, et al., Coord. Chem. Rev. 449 (2021) 214216.
[21] T. Zhao, X. Wang, Z. Sun, et al., Adv. Funct. Mater. 33 (2023) 2303644.
[22] T. Tsuruoka, S. Furukawa, Y. Takashima, et al., Angew. Chem. Int. Ed. 48 (2009) 4739.
[23] C. Atzori, G. Shearer, L. Maschio, et al., J. Phys. Chem. C 121 (2017) 9312–9324.
[24] E. Bagherzadeh, S. Zebarjad, H. Hosseini, Eur. J. Inorg. Chem. 2018 (2018) 1909–1915.
[25] D. Jiang, Y. Zhu, M. Chen, et al., Appl. Catal. B: Environ. Energy 255 (2019) 117746.
[26] Z. Xu, R. Teng, L. Xu, et al., Adv. Funct. Materials 34 (2024) 2401248.
[27] H. Chen, J. Wan, Z. Yan, et al., J. Clean. Prod. 348 (2022) 131367.
[28] J. Łuczak, M. Kroczewska, M. Baluk, et al., Adv. Colloid Interface Sci. 314 (2023) 102864.
[29] C. Marshall, E. Timmel, S. Staudhammer, et al., Chem. Sci. 11 (2020) 11539–11547.
[30] D. Bara, E. Meekel, I. Pakamorė, et al., Mater. Horiz. 8 (2021) 3377–3386.
[31] P. Coliaie, R. Bhawnani, A. Prajapati, et al., Lab Chip 22 (2022) 211–224.
[32] T. Rayder, A. Bensalah, B. Li, et al., J. Am. Chem. Soc. 143 (2021) 1630–1640.
[33] H. Liu, L. Chang, C. Bai, et al., Angew. Chem. Int. Ed. 55 (2016) 5019.
[34] M. Sha, L. Rao, W. Xu, et al., Nano Lett. 23 (2023) 701–709.
[35] M. Sha, W. Xu, Y. Wu, et al., Sens. Actuators B: Chem. 366 (2022) 131927.
[36] R. Tuttle, R. Daly, C. Rithner, et al., ACS Appl. Mater. Interfaces 13 (2021) 52006–52013.
[37] L. Fang, Y. Zhang, H. Ding, et al., Adv. Funct. Mater. 34 (2024) 2309338.
[38] W. Zhang, D. Sun, B. Yang, et al., Chem. Eng. J. 507 (2025) 160645.
[39] S. Niu, D. Yue, H. Wang, et al., ACS Appl. Mater. Interfaces 16 (2024) 36295–36303.
[40] C. Wen, S. Yang, J. He, et al., Small 20 (2024) 2405051.
[41] N. Rathod, S. Mishra, S. Mishra, et al., Chem. Eng. J. 477 (2023) 146765.
[42] J. Xie, X. He, K. Liu, et al., Sep. Purif. Technol. 351 (2024) 128043.
[43] W. Zhang, B. Lucier, V. Terskikh, et al., Chem. Sci. 15 (2024) 6690–6706.
[44] Y. Fu, Y. Yao, A. Forse, et al., Nat. Commun. 14 (2023) 2386.
[45] Z. Karimi, B. Karami, M. Farahi, et al., Mater. Today Chem. 38 (2024) 102085.
[46] W. Xu, N. Hanikel, K. Lomachenko, et al., Angew. Chem. Int. Ed. 62 (2023) e202300003.
[47] Y. Cai, Y. Wu, Y. Tang, et al., Small 20 (2024) 2403354.
[48] Y. Wu, Y. Tang, W. Xu, et al., Small 19 (2023) 2302929.
[49] Y. Yang, C. Tong, R. Zhou, et al., Food Chem. 431 (2024) 137127.
[50] J. Chang, L. Yu, T. Hou, et al., Anal. Chem. 95 (2023) 4479–4485.
[51] Q. Liu, S. Li, Y. Wang, et al., Sci. Total Environ. 882 (2023) 163548.
[52] X. Cheng, Y. Xie, G. Li, et al., Inorg. Chem. Front. 10 (2023) 2335–2343.
[53] Y. Huang, Z. Li, K. Yao, et al., Appl. Catal. B: Environ. Energy 299 (2021) 120671.
[54] H. Wang, R. Sun, P. Liu, et al., Nano Res. 17 (2024) 7013–7019.
[55] S. Siddiqui, J. Niazi, A. Qureshi, Mater. Today Chem. 22 (2021) 100560.